www.czasopisma.pan.pl PAN POLSKA AKADEMIA NAUK www.journals.pan.pl

Arch. Min. Sci. **68** (2023), 3, 425-441

Electronic version (in color) of this paper is available: http://mining.archives.pl

DOI: https://doi.org/10.24425/ams.2023.146860

JAKUB JANUS[1*], JERZY KRAWCZYK[1]

DEFINING THE COMPUTATIONAL DOMAIN AND BOUNDARY CONDITIONS FOR FLUID FLOW IN A MINING EXCAVATION

For underground mine workings, the shape of the computational domain may be difficult to define. Historically, the geometry models of mine drifts were not accurate representations of the object but rather a simplified approximation. To fully understand a phenomenon and save time on computations, simplification is often required. Nevertheless, in some situations, a detailed depiction of the geometry of the object may be necessary to obtain adequate simulation results. Laser Scanning enables the generation of 3D digital models with precision beyond the needs of applicable CFD models. Images composed of millions of points must be processed to obtain geometry suitable for computational mesh generation. A section of an underground mine excavation has been selected as an example of such transformation. Defining appropriate boundary conditions, especially the inlet velocity profile, is a challenging issue. Difficult environmental conditions in underground workings exclude the application of the most efficient and precise methods of velocity field measurements. Two attempts to define the inlet velocity profile have been compared. The first one used a sequence of simulations starting from a flat profile of a magnitude equal to the average velocity. The second one was based on the sixteen-point simultaneous velocity measurement, which gave consistency with measurement results within the range of applied velocity measurement method uncertainty. The article introduces a novel methodology that allows for more accurate replication of the mine excavation under study and the attainment of an appropriate inlet velocity profile, validated by a satisfactory correspondence between simulation outcomes and field measurements. The method involves analysing laser-scanned data of a mine excavation, conducting multi-point velocity measurements at specific cross-sections of the excavation that are unique to mining conditions, and utilising the k-ω SST turbulence model that has been validated for similar ventilation problems in mines.

Keywords: CFD; mine ventilation; numerical model geometry; laser scanning; velocity profile; boundary conditions

[1] STRATA MECHANICS RESEARCH INSTITUTES OF POLISH ACADEMY OF SCIENCE, 27 REYMONTA STR., 30-059 KRAKÓW, POLAND

* Corresponding author: janus@imgpan.pl

1. Introduction

Safe and efficient ventilation of underground mines requires vast and precise knowledge of several flow phenomena. Application of Computational Fluid Dynamics methods may provide images of flow phenomena which could solve several problems [25,31]. Compared with many laboratory or industrial problems, research on flow in the workings of underground mines faces additional difficulties with defining computational domain and boundary conditions. The initial task involves generating a geometric model that accurately reflects the geometry of the mine drift. Even perfectly cut shapes deform due to subsidence in an erratic manner [6]. When using standard measurement tools such as a meterstick or laser rangefinder, it can be extremely challenging to map out certain features of underground mine conditions, such as intersections between mine drifts, floor uplifts, mine drift convergence, the deformation of arch-yielding supports, the uneven placement of arch-yielding supports, and the presence of mining equipment like belt conveyors, shearers, or pipelines [32]. Consequently, current research utilising CFD methods to examine air flow issues in underground settings is based on mine drift models that are not accurate reflections of the actual object but rather rough approximations. A commonly used technique for simplifying models is assuming a uniform geometry throughout its entire length. This approach is often necessary for obtaining a clear understanding of the phenomenon under investigation and expediting the development of the model and numerical calculations. However, it is essential to evaluate the impact of these simplifications on the accuracy of the calculated results.

Therefore we need an exact representation of geometry as a reference. For underground mine conditions acquisition of sufficiently precise data with the classic measurement methods is practically impossible. Fortunately, the new LiDAR scanning methods, which have become popular for the acquisition of digital 3D models of various structures, can also be applied in underground mine workings [28], in remediation of grassland subsidence [4] or in Solar Potential Analysis [23].

Another obstacle in creating guidelines for numerical simulation for the mine environment is the problem of boundary conditions [5,33]. Profiles of the turbulent developed flow for regular shapes such as round or rectangular pipes have been known for a long time. Drifts with arch-yielding support are common in underground mines [8]. For flow analysis, such excavation is a specific kind of closed conduit with ribbed walls [15]. The cross-section of a mine drift with arch-yielding support may be calculated by empirical method or approximated by a semi-ellipse.

The most frequently used method for calculating cross-sectional areas in underground mining, the empirical method, involves measuring the mine drift's height & width and multiplying their product by 0.8 [26]. The value 0.8 results from the shape of the arch yielding support and is therefore called the cross-sectional shape coefficient. The height of the mine drift is measured in the middle of the drift's width, from the highest point on the arch to the corresponding point on the floor. The width is measured by placing measuring points on the straight section of the side part of the arch. In some cases, just a part of the straight section is above the floor, and occasionally this straight section is much shorter or completely inaccessible, making it difficult to perform the measurement properly and increasing the uncertainty of the result.

$$A_g = 0.8 \cdot H \cdot W \tag{1}$$

where:

H — height of mine drift,
W — width of mine drift.

Comparing the equations for the empirical method and the method based on approximation by a semi-ellipse, it is readily seen that they differ only in the cross-sectional shape coefficient: for the empirical method the coefficient is 0.8, and for approximation by a semi-ellipse the coefficient is 0.785.

At many measuring sites, it is found that a coefficient lower than 0.8 is more accurate in calculating the cross-sectional area. This applies to places with high rock stress, such as in walls. The relationship between the floor height and the cross-sectional shape coefficient is shown in the graph below. The floor height is the depth of the arch's side part in the floor.

Initially, the arch-yielding supports have been arranged in a regular manner (constant distance). The walls between them form a so-called lining, usually from concrete blocks or steel mesh. Inevitable pressure of the surrounding strata causes subsidence and an erratic deformation of the walls. Cracked rocks form a porous medium that can participate in the flow depending on the lining's impermeability and rock permeability. Each of these elements impacts the velocity profile shape in mine drift, which is very difficult and in some cases, even impossible to map without dedicated precise measurements.

A realistic inlet velocity profile is crucial for accurate CFD modelling of flow in drifts. This work is trying to present a new way of generating boundary conditions for CFD modelling in a mining environment. For over ten years, scientists using CFD methods for mine ventilation problems were struggling with generating inlet velocity profile problems. In many cases, only a flow rate and drift geometry are available. Authors have selected a flow in a drift's fragment as a test case to see if a method of application of a developed velocity profile to the inlet of a not-too-long section of a drift would provide a sufficiently accurate velocity profile at its end. The authors intend to show that the extension of scanned mine drift by an inlet section of a moderate length pays off by providing space for the generation of a sufficiently realistic velocity profile in cases when only a flow rate is available.

2. Development of the computational domain upon the Laser Scanning

The FARO Focus 3D laser scanner was utilised for assessing the geometry of the excavation mine drift. This compact instrument measures $0.24 \times 0.20 \times 0.10$ m in dimensions and weighs a total of 5 kg. With a range spanning from 0.6 m to 120 m, the scanner emits a laser beam at a 90° angle towards a surface with 90% reflectance. Remarkably, the scanner boasts a rapid measurement speed, ranging from 120,000 points per second to 976,000 points per second, contingent upon the scan resolution. The measurement error is ±0.002 m. Its visual field encompasses a full 360° in the horizontal plane and 305° in the vertical plane. The laser power is 20 mW, operating at a wavelength of 905 nm, and featuring a typical beam divergence of 0.16 mrad.

The chosen section for analysis is the Grodzisko crosscut within the Sobieski coal mine, which comprises two nearly straight segments linked by a curved section secured with 8-KS/KO-21 type arch supports. In this zone, a set of six laser scans has been performed, providing consistent data in the form of 152 million points located at the walls and floor of excavation and surfaces of several devices placed inside, like arches of the yielding support pipelines and cables (Fig. 1).

Building the geometry for the computational mesh generation required reverse engineering transformation of this data in three steps:

- step 1 – reducing the obtained point cloud, clearing it of redundant elements, and separating individual elements such as arch support, floor, pipelines
- step 2 – triangulation of the point cloud to create a CAD model in reverse engineering software e.g. Geomagic Wrap
- step 3 – designing a 3D model based on the obtained CAD model in e.g. Solidworks software

This process is described by Janus [11]. Due to the small diameter of the cables, they were not included in the numerical geometry model.

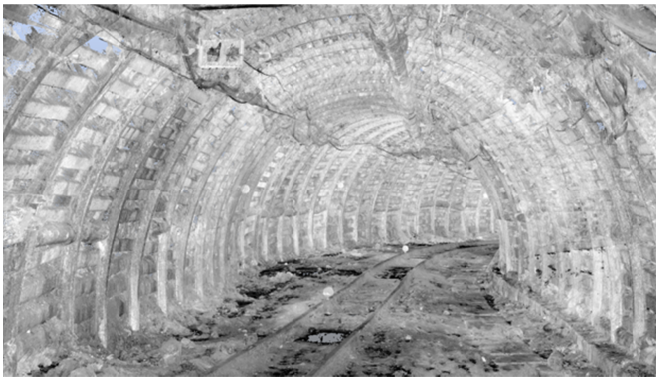

Fig. 1. Point Cloud

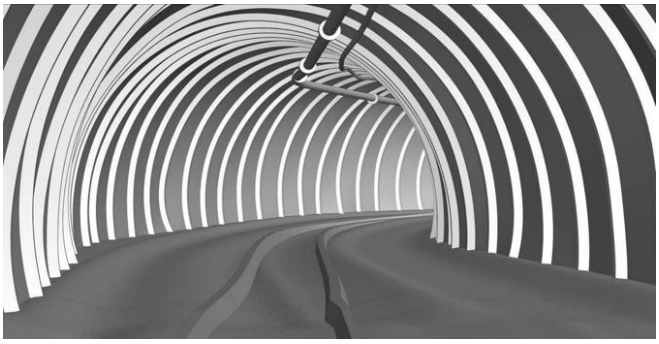

Fig. 2. Numerical geometry model

Automated image processing techniques have been successfully used to evaluate basic domain parameters such as volume [29]. However, generating a volume suitable for CFD meshing software has not yet been achieved through automation. That is why the boundary of the domain has been manually drawn using the cloud of points as a template. The geometry model contains the hydraulic conduits and pipeline near the roof, deformation of the floor and individual

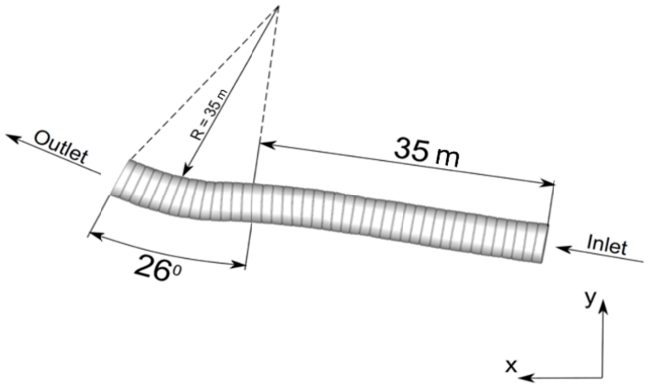

Fig. 3. Dimensioning of the numerical geometry model

arch-yielding supports (Fig. 2). Distance between yielding supports was 1 m. of the curve with a 35-metre turning radius and a 26-degree turning angle (see Fig. 3). The initial portion of the mine drift had an almost straight axis with only variations in cross-sectional shape. In the following section, the mine drift curved to the right with a 35-metre radius.

3. Cross-sectional velocity field measurements

Specific environmental conditions of underground workings limit the scope of devices applicable for the measurement of velocity fields. So far, nobody was able to apply Particle Image Velocimetry in underground mines. It is possible to get a limited number of point velocity measurements. The velocity range of 2 m/s is too low for the application of the Pitot-Prandtl tubes or similar devices. Another option was the hot wire anemometers. There have been some successful applications of hot wire probes, which have survived in a dusty and humid atmosphere providing valuable data not only on the average but also fluctuation properties of velocity. During measurements a set of four probes measuring simultaneously was available. Measuring the velocity field in the entire cross-section would require subsequent measurements in several probing lines. As measurements in three cross-sections had to be planned within a few hours of the availability of the place, this method was rejected as too time-consuming. Another factor was the eventual unsteadiness of velocity in this work, which would require simultaneous multipoint measurements at whole cross-sections. For underground mine ventilation, the vane anemometers are the most suitable velocity sensors. They have proven to be reliable in difficult environmental conditions. Some versions even may operate in gas explosion hazard zones. The unique mining conditions permitted the use of a custom-designed multipoint system for measuring flow velocity based on vane anemometers (named SWPPP) [19]. The SWPPP records the flow velocity at 16 to 20 points in a synchronous way.

Simultaneous measurement was possible with a set of 16 in-house developed vane anemometers SOM 2303, designed and produced in Strata Mechanics Research Institute. They have been placed in a plane of a selected cross-section on four pillars of a scaffold (Fig. 4). This set provides data on the velocity with a frequency of 1 Hz with flow reversal detection [21].

The uncertainty has been evaluated by Krach [18]. The velocity recordings show significant fluctuations hence those sensors, despite their mechanical inertia, can provide some image of turbulence for the frequency range encountered in flow in such galleries. This data has been supplemented with results of turbulence measurements done earlier in similar conditions with the hot wire sensors. Due to their directional characteristics, the vane anemometers should be oriented in parallel to the flow direction. Therefore they have been placed in a straight section, where the dominant velocity should be parallel to the excavation axis.

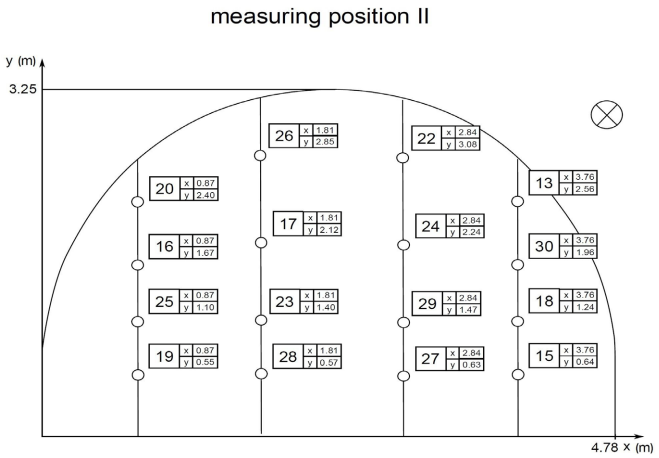

Fig. 4. Anemometer sensor locations on the measuring cross-section

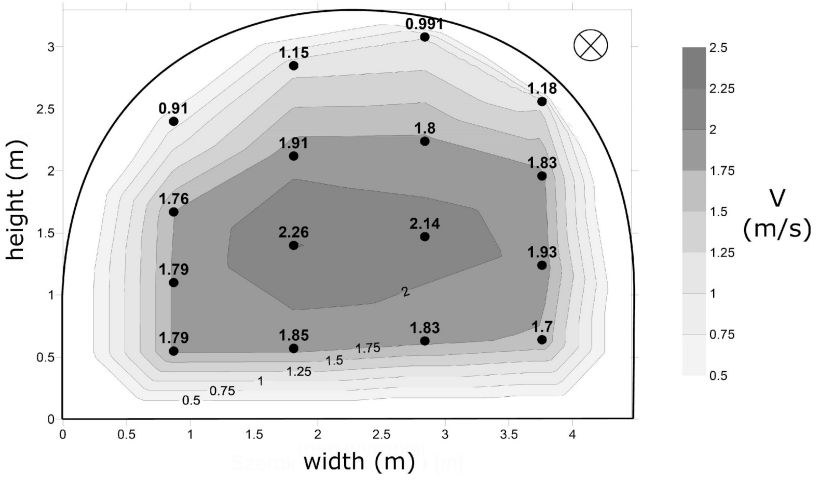

Fig. 5. Isolines of velocity in the measurement cross-section

To analyse the flow in a bend, a location 3 metres before the entrance of the bend was selected. Prior to the bend, from the inflow side, there was a straight section of the mine drift

approximately 500 metres long. The measured dimensions of the cross-section were 4.78 metres wide and 3.25 metres high. The arch-yielding supports were spaced at 1-metre intervals (Fig. 4).

To simplify the visualisation of the airflow in the cross-section, it was determined to display the mean measured air velocity in the form of isolines (Fig. 5). The velocity distribution isolines were created using gridding estimation, employing the triangulation method in conjunction with linear interpolation. By examining the airflow visualisation in the cross-section, a well-developed profile of the airflow was observed. A velocity profile with such a shape was obtained thanks to a 500-metre straight section of the mine drift preceding the measuring cross-section. The profile was disturbed at the inlet to the mine drift section due to the intersection, but along this straight section, the velocity profile was formed due to the tangential forces from the fluid layers in the immediate vicinity of the arch-yielding supports, transferred to layers closer to the axis of the mine drift.

4. Numerical research

4.1. Grid generation

The geometry of the calculated geometry model justified the implementation of a dense computing mesh. It was decided to use the size function mesh control in ANSYS Meshing software, which allows control of the size of a mesh around a selected point, edge or surface. A grid sensitivity study was carried out in a similar way presented in the article [12]. The method involved designing three computational grids with greater density, performing numerical calculations on them, and then comparing velocity components for a selected segment. After conducting the analysis, a grid size was chosen for which the results deviated less from the denser grid. A numerical model has been digitised with the unstructured tetrahedral mesh consisting of 13 million cells, which then, due to the large size of the model and selection of a dense computing mesh, was converted into a polyhedral mesh. After conversion the number of cells decreased to 2.1 million polyhedral cells (Fig. 6). This conversion from tetrahedral to polyhedral mesh

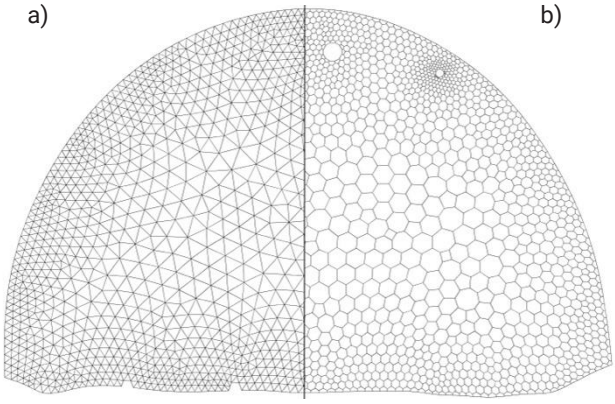

Fig. 6. Inlet cross-section computational mesh:
a – Tetrahedral grid, b – Polyhedral grid obtained after conversion

reduces the number of cells, reduces skewness and improves the mesh quality. A major advantage of polyhedral cells is that they have many neighbours (typically of order 10), so gradients can be sufficiently approximated.

For the given grid density, the dimensionless length parameter y^+ for the computational domain is within the range of $10 \leq y^+ \leq 500$. The number of cells within the range of $10 \leq y^+ \leq 40$ is small, which indicates good grid quality in terms of the dimensionless length parameter y^+ [20].

4.2. Generation of the inlet boundary condition

The profile based on 16 points plus zero velocity at the boundary is too rough for the conditions at the inlet to a computational domain. The authors needed to obtain a denser velocity profile that matched the measured data. To achieve this, they conducted two numerical simulations with different boundary conditions at the inlet of the numerical model:

- developed profile from average velocity $v = 1.6$ m/s,
- velocity profile obtained from measured data and additional points.

In both cases, an artificial computational domain has been created at the inflow side of the place of velocity measurement.

Due to the characteristics of the airflow in the mine excavation, the k-ω SST turbulence model [2,22] was selected for numerical calculations. To create more realistic flow conditions at the inlet, a vortex generator was used. Unsteady flow calculations with a time step of 0.01 s were applied, and solutions converged after fewer than 20 iterations per time step. The residuals for continuity were below 1×10^{-5} and even smaller for other variables. The suggested methods for *k-ω* SST turbulence model solutions, such as second-order pressure and bounded central differencing for the transient formulation, were utilised. The calculations for each model were carried out until the time-averaged values stabilised. Then, the averaging was restarted and the new average was used for comparisons. The initial calculations were performed for a few multiples of the flow passage time.

The inlet boundary condition for the model was set as velocity inlet, with defined velocity profiles. The velocity inlet boundary condition does not keep the total pressure constant, but it is adjusted to ensure a specific velocity distribution.

For each case, the outflow boundary condition was applied to the outlet, using the outflow model, which does not specify the velocity or pressure conditions. The floor, arches, rails, and pipelines were designated as wall surfaces in the simulation. Surface irregularities on the floor were represented as roughness with a height of 0.05 m, while arches, rails, and pipelines were assigned a roughness height of 0.001 m.

4.2.1. A method of the inlet profile generation based on the average velocity

A traditional option would be to create an artificial inlet. It is made by extruding the shape of the cross-section at the place of measurements from the geometric model shown in Fig. 3, obtained using laser scanning. At the inlet of such a section, a flat velocity profile of a magnitude equal to the average of the actual velocity has been applied. If the section is long enough at its outlet, the developed velocity profile should appear [3,24,34]. Another option is to solve a steady-state

flow problem with periodical velocity conditions. The authors used a sequence of solutions for a 30 m long section of a constant area of 11.28 m^2 and the shape identical to the measuring section (Fig. 9). The initial scenario involved implementing a level profile with a constant velocity of v = 1.6 m/s. The intensity of turbulence was defined based on measurements of flow velocity in a mine excavation using PT100 thermo anemometers [27]. The resulting outlet profile has been used as an inlet one for the next computation. This sequence has been repeated four times when the inlet and outlet profiles became sufficiently similar, which is an analogy of a single 120-long section (Fig. 7).

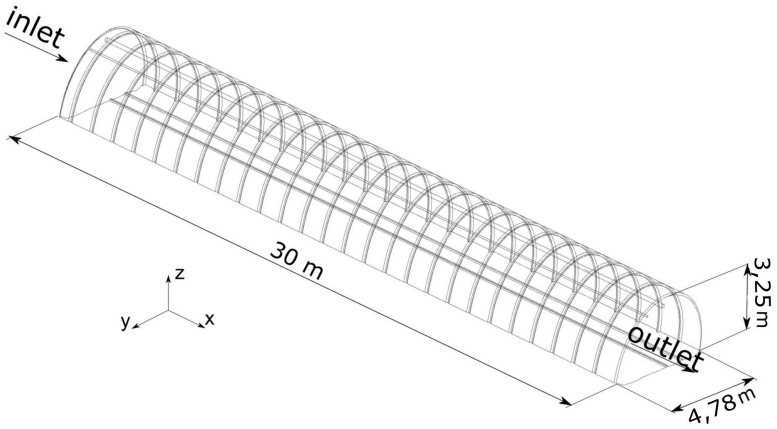

Fig. 7. Section of mine drift for profile generation

4.2.2. A method of the inlet profile generation based on the 16-point velocity measurement

The whole method of calculating the velocity field using the SWPPP multipoint system of flow velocity measurements is described in monography [19]. In this work, the authors present a new way of calculating the velocity field and volumetric flow rate using vane anemometers placed in the cross-section of a mine drift. To calculate the volumetric flow rate, the cross-section of a mine drift, where the measurement takes place, the velocity profile needs to be integrated. In reality, it is impossible to measure the whole velocity field in a cross-section. That is why, the flow velocity is measured in a finite number of points on this surface and then, based on the results, the velocity distribution is estimated using linear triangulation. This method consists in dividing the cross-section area into triangular areas so that the vertices of the triangles are points at which the flow velocity is known from the measurements.

The low accuracy of the first attempt at generating the profile (Fig. 8) prompted the authors to apply a profile roughly interpolated on the measured values. The velocity measurements provided data that could be used as a boundary condition at the inlet. To augment the defined profile, 31 additional points were inserted between the measured points. The triangulation method with linear interpolation was used to determine velocity values at the additional points.

The imported profile and the additional points were then subjected to the zero-order interpolation process in the numerical program, resulting in the inlet profile (Fig. 9).

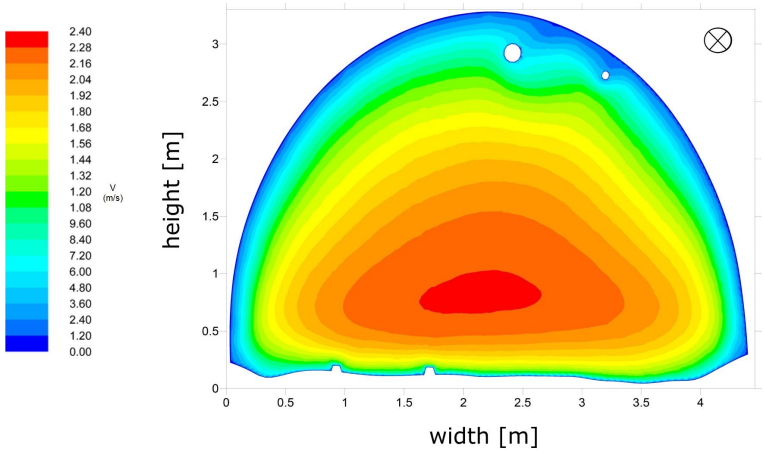

Fig. 8. Developed velocity profile from average velocity

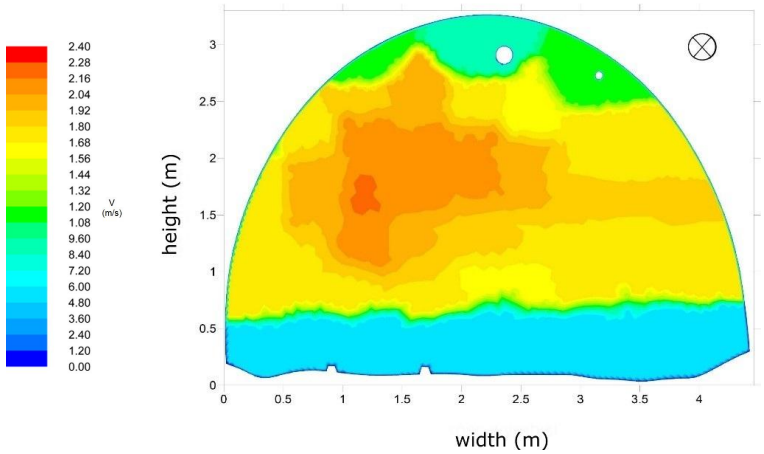

Fig. 9. Obtained velocity profile by combining the data from the measurements and the additional points

5. Discussion of the simulation results

For further CFD calculations on the numerical geometry model designed using Laser Scanning (Fig. 3), both profiles have been used as a boundary condition. To facilitate a qualitative evaluation of the simulation results, velocity contours were generated for the measuring cross-section of the geometry located 32.0 m downstream from the inlet of the numerical model. The contours were presented on the same scale (Fig. 10).

Furthermore, average velocity values for each measuring point (corresponding to the anemometer position in the measuring cross-section) were tabulated, including values obtained from both measurements and CFD simulations.

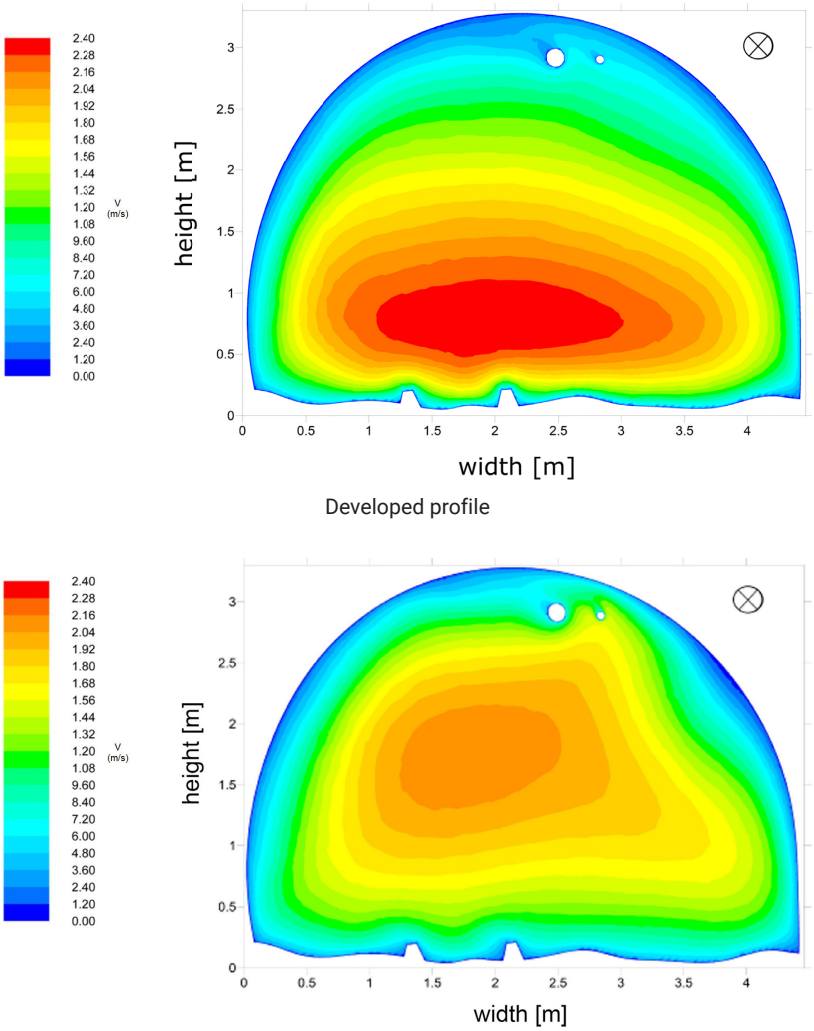

Fig. 10. Velocity contours plotted for velocity inlet profiles in the measuring cross-section

To provide a quantitative evaluation of the accuracy of the numerical simulations, a relative error measure [12] was utilised.

$$\delta = \frac{\Delta x}{x} \cdot 100\% = \frac{|x - x_0|}{x} \cdot 100\% \tag{2}$$

where:

x — measured quantity,

x_0 — quantity computed numerically.

To determine the average relative error for the entire measuring cross-section, the sum of relative errors at each individual measuring point is divided by the total number of measuring points:

$$\delta_{śr} = \frac{1}{n}\sum_{i=1}^{n}\frac{|x - x_0|}{x}\cdot 100\% \tag{3}$$

where: n — number of measuring points in the cross-section.

TABLE 1 presents a comparison between the numerical computation results and the results obtained from the measurements, along with the calculated relative error for each measuring point. One important aspect to note is the difference in the average relative error between the profile obtained through measurements and the one simulated numerically. The result of an average relative error of 11.7% for the measurement-based profile appears to be significantly lower than the result of 27.2% for the profile developed based on numerical simulations. This suggests that the numerical simulations may be subject to higher errors when compared to the actual measurements. When the inlet profile data is unavailable, the developed profile calculations described earlier are used to generate it. However, it should be noted that the calculation of the expanded profile does not consider the impact of various factors occurring on the inflow side of the inlet cross-section, which may affect the inlet velocity profile. The information presented in TABLE 1 enables us to evaluate the extent to which the accuracy of the calculations diminishes when the inlet boundary condition is unknown. Fig. 11 presents a comparison of measured velocities with

TABLE 1

Comparison between the numerical computation results and the results obtained from the measurements, along with the calculated relative error for each measuring point

Anemometer sensor no	Developed profile			Anemometer sensor no	Profile from measurements		
	V_{av} [m/s]		relative error [%]		V_{av} [m/s]		relative error [%]
	SWWPP	CFD			SWWPP	CFD	
13	1.18	0.51	56.7	13	1.18	0,58	50,5
15	1.7	2.09	22.6	15	1.7	1,6	6,19
16	1.76	1.55	11.9	16	1.76	1,8	2,43
17	1.91	1.38	27.8	17	1.91	2.0	4,72
18	1.93	1.71	11.5	18	1.93	1.66	14.0
19	1.79	2.25	25.6	19	1.79	1.66	7.4
20	0.91	0.74	18.7	20	0.91	0.91	0.0
22	0.99	0.47	52.6	22	0.99	1.01	1.6
23	2.26	2.01	11.1	23	2.26	2.09	7.43
24	1.8	1.2	33.4	24	1.8	1.9	5.39
25	1.79	2.02	12.6	25	1.79	1.82	1.75
26	1.15	0.68	40.9	26	1.15	1.0	13.0
27	1.83	2.33	27.1	27	1.83	1.54	15.7
28	1.85	2.38	28.9	28	1.85	1.63	11.9
29	2.14	1.82	14.9	29	2.14	1.96	8.34
30	1.83	1.11	39.3	30	1.83	1.12	39.0
	mean relative error [%]		27.2		mean relative error [%]		11.7

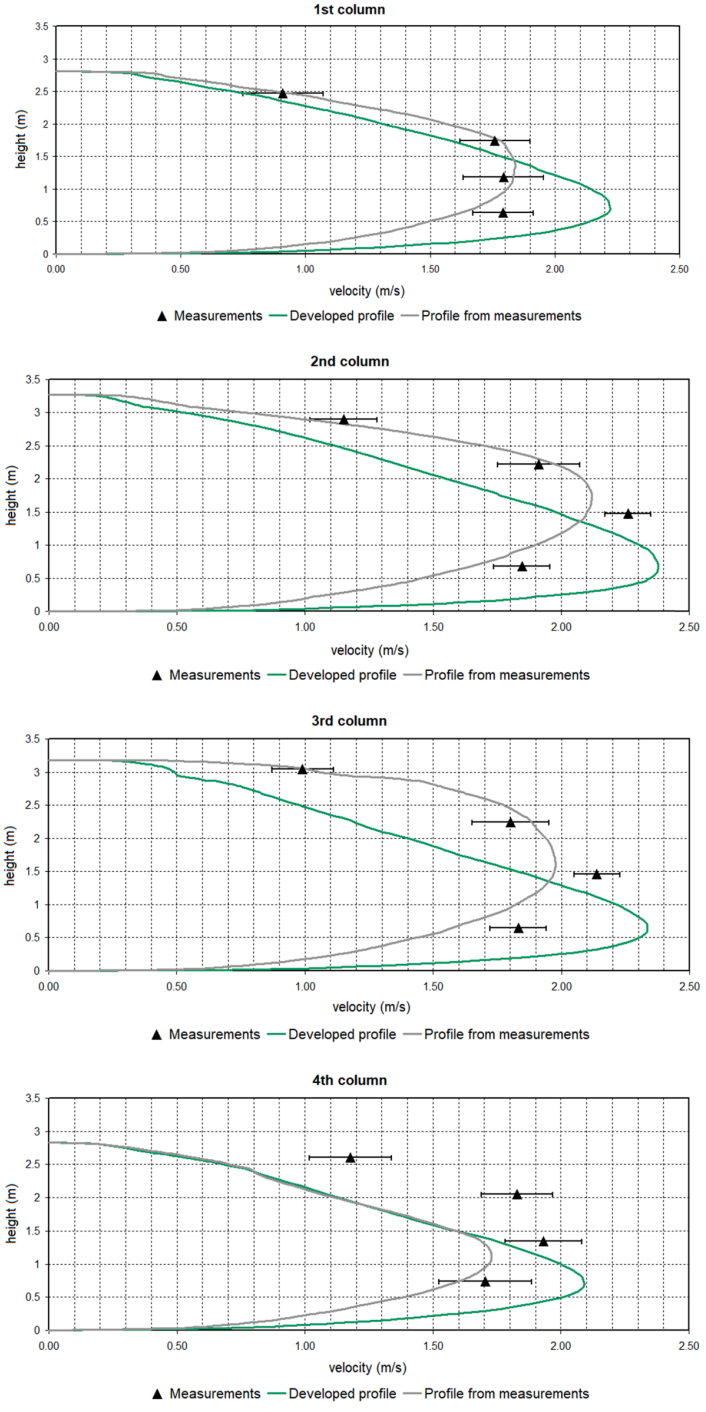

Fig. 11. Comparison of airflow measurements with calculated velocities

calculated velocity profiles for four vertical measurement lines. Anemometer measurement results include the measurement uncertainty, calculated according to the formula provided by the producer. Scaffold's column numbers correspond to the following columns, counting them from the left side (the side of the side wall in the direction of airflow). Figures take into account the average measured velocities along with the standard deviations for individual measurement points.

Based on the provided information, it can be observed that there is a noticeable difference in the average relative errors between the measurement-based profile and the profile developed based on numerical simulations. The lower average relative error for the measurement-based profile suggests a closer agreement with the actual measurements compared to the profile generated through numerical simulations.

In the analysis of the results, it is equally important to consider sources of measurement errors and errors arising from numerical simulations. Utilising only 16 anemometric sensors does not provide a complete picture of the air velocity profile in the investigated excavation, being an estimation of the measured results. However, even this number of point data provides a considerably larger accuracy (TABLE 1 and Fig. 11)

The numerical simulation also carries errors stemming from factors such as the choice of turbulence model. In the calculations, the k-ω SST model was employed, which combines the advantages of the k-e and k-ω models while introducing an additional term to restrict the excessive production of the kinetic energy of turbulence in areas with strong positive pressure gradients (constriction points, boundary layer separation regions). This model has proved to provide accurate results for CFD simulations in mining excavations [16,17].

While the k-omega SST model has many advantages, there are also certain limitations and drawbacks to consider. Here are a few examples:

1. Grid sensitivity: The k-omega SST model can be sensitive to the quality of the numerical grid. Inaccurate or unstable grids can lead to incorrect results or convergence difficulties. Compared to other models, the k-omega SST model may require more careful grid matching to obtain accurate results.
2. Wall-layer modelling: Although the k-omega SST model is relatively well-suited for wall-bounded flows, it may not perform optimally in highly separated or low-flow regions near walls. In such cases, more advanced models or techniques may be required.

It is important to note that the choice of an appropriate turbulence model depends on the specific nature of the problem, flow conditions, and available computational resources. In the case of performing numerical simulations of airflow in a mine environment, the k-omega model gives satisfactory results and allows for much shorter calculation times, e.g. compared to the SAS turbulence model.

6. Conclusion

Underground mine galleries are a common feature, but the areas that pose the most difficulties for mine ventilation are elsewhere. Among them, the closest one is a development heading. The galleries are cut in the strata. The blind end of an excavation, where rocks are cut or blasted is the development heading. In this zone, several ventilation-related problems occur, like prevention from the accumulation of explosive gases, dust or too hot a climate. On the other hand, the

solution to those problems requires a basic knowledge of the velocity profile at the boundary of this zone, which is a straight excavation.

Longwall is another problematic zone [15,30]. For this way of extraction, the excavated rock, most often coal, is cut slice by slice on a long rectangular surface [7]. The coal face is surrounded by a complex system of devices for support of surrounding strata, cutting and coal transport. But often, at the inlet and outlet of this system, there are arched galleries. Those examples show that the problem presented in this paper, although basic, provides a valuable foundation for further studies.

This paper presents a methodology that integrates laser scanning, multipoint velocity measurements, and a validated turbulence model. It addresses the challenges encountered in mine ventilation, particularly in areas such as the development heading and longwall zones, where various ventilation-related issues arise. The experiment described in the paper involves the simultaneous use of laser scanning and flow measurements, enabling the analysis of the actual domain geometry at a later stage. This knowledge of the excavation gallery's true shape becomes instrumental in selecting appropriate velocity measurement sites.

The paper introduces a novel approach for obtaining the inlet velocity profile without the need for extensive multipoint probing of the velocity field. Instead, the relevant profile is derived from information on the inlet flow rate, coupled with the introduction of highly precise geometry obtained through laser scanning. This method effectively applies a developed inlet velocity profile to an excavation gallery with an exact geometry spanning eight hydraulic diameters. The accuracy of this approach is tested against multipoint velocity measurements used as a reference.

Furthermore, previous comparisons of calculations performed with approximate and accurate geometries, as documented in the referenced PhD thesis [10], have demonstrated that incorporating the precise geometry of the investigated area can enhance calculation accuracy by approximately 40%.

The paper also emphasises the necessity of developing efficient methods for laser scanning applications. Until recently, there were no automated means of transforming point cloud data into a CFD meshable geometry which required laborious manual work. However, recent advancements in automated processing, as highlighted in relevant literature [1], provide hope for overcoming this limitation and facilitating easier access to precise geometries. The paper underscores the importance of exploring more efficient ways of applying laser scanning and transforming point cloud data into CFD geometries, capitalising on these promising advancements in automated processing.

In the experiment described in this paper, the laser scanning was made simultaneously with the flow measurements. Due to a proper sequence of positioning of the laser, the velocity measurement was not disturbed. Analysis of the actual geometry of the domain could be done much later, after a time-consuming post-processing. Knowledge of the actual shape of the excavation may lead to a better selection of the sites of velocity measurement.

In comparison with an average velocity measurement, the multipoint velocity measurement is much more complicated and requires special equipment. Additional flow studies based on the geometry obtained from laser scanning could provide more comprehensive insights into using actual inflow geometry information to generate appropriate inflow conditions at the domain's inlet [14].

This paper presents a part of a study on the sensitivity of solutions to the precision of geometry representation. The first results of this analysis have been shown in a work [10]. Some of the ideas presented in this paper have been discussed at the Fluid Mechanics Conference [13].

Acknowledgements

This paper presents the results of the statutory research of the Strata Mechanics Research Institute of the Polish Sciences Academy in the years 2017–2018.

References

[1] H. Bouchiba, S. Santoso, J.E. Deschaud, L. Rocha-Da-Silva, F. Goulette, T. Coupez, Computational fluid dynamics on 3D point set surfaces. Journal of Computational Physics **7** (2020). DOI: https://doi.org/10.1016/j.jcpx.2020.100069

[2] M. Branny, M. Karch, W. Wodziak, M. Jaszczur R. Nowak, J.S. Szmyd, An experimental validation of a turbulence model for air flow in a mining chamber. Journal of Physics: Conference Series 530 (2014). DOI: https://doi.org/10.1088/1742-6596/530/1/012029

[3] D. Cardwell, P. Vlachos, K. Thole, Developing and fully developed turbulent flow in ribbed channels. Experiments in Fluids **50** (2011). DOI: https://doi.org/10.1007/s00348-010-0993-y

[4] X. Chen, L. Gua, W. Xu, Y. Zhao, Remediation of grassland subsidence and reduction of land occupation with tailings backfill technology: a case study of lead-zinc mine in Inner Mongolia, China. Front. Environ. Sci. **11**, 1183945, (2023). DOI: https://doi.org/10.3389/fenvs.2023.1183945

[5] N.S. Dhamakar, G.A. Blasdell, A.S. Lyrintzis, An Overview of Turbulent Inflow Boundary Conditions for large Eddy Simulations. Proc of the 22nr AIAA Computational Fluid Dynamics Conference AIAA Paper (2015).

[6] S. Duży, Zachowanie się odrzwi stalowej obudowy podatnej w warunkach deformacyjnych ciśnień górotworu w świetle obserwacji dołowych. Górnictwo i Geoinżynieria **31**, 3 (2007).

[7] W. Dziurzyński, A. Krach, J. Krawczyk, T. Pałka, Numerical Simulation of Shearer Operation in a Longwall District. Energies **13**, 5559 (2020). DOI: https://doi.org/10.3390/en13215559

[8] P. Horyl, P. Maršálek, R. Šňupárek, Z. Poruba, K. Pacześniowski, Parametric Studies of Total Load-Bearing Capacity of Steel Arch Supports. Acta Montanistica Slovaca **24**, 3 (2019).

[9] J. Janus, Air flow modelling on the geometry reflecting the actual shape of the longwall area and goafs. Archives of Mining Sciences **66** (2021). DOI: https://doi.org/10.24425/ams.2021.139593

[10] J. Janus, Modelling of flow phenomena in mine drifts using the results of laser scanning. Ph.D. thesis, in Polish, Strata Mechanics Research Institute of Polish Academy of Sciences (2018).

[11] J. Janus, The Application of laser scanning in the process of constructing a mine drift numerical model. 24th World Mining Congress PROCEEDINGS – Underground Mining, Brazilian Mining Association, Rio de Janeiro (2016).

[12] J. Janus, J. Krawczyk, Measurement and simulation of flow in a section of a mine gallery. Energies **14**, 4894 (2021). DOI: https://doi.org/10.3390/en14164894

[13] J. Janus, J. Krawczyk, An example of defining boundary conditions for a flow in a mine gallery. Abstract in the XXIII Fluid Mechanics Conference Materials, Zawiercie, 9-12 September 2018 (2018).

[14] J. Janus, J. Krawczyk, Modeling velocity fields of air flow in the mine galleries with arc roof support – selected issues. Monograph, Strata Mechanics Research Institute of Polish Academy of Science (2016).

[15] J. Janus, J. Krawczyk, The numerical simulation of a sudden inflow of methane into the end segment of a longwall with Y-type ventilation system. Archives of Mining Sciences **59**, 4 (2014).

[16] J. Janus, J. Krawczyk, Velocity Field infthe area of artificially generated barrier on the mine drift floor. Przegląd Górniczy, No 11 (2015).

[17] J. Janus, J. Krawczyk, Velocity field in thein the corners and intersection of mine drifts. Przegląd Górniczy **11** (2015).

[18] A. Krach, Uncertainty of measurement of selected quantities in mine ventilation measurements. Archives of Mining Sciences, Series: Monograph 8 (2009).

[19] A. Krach, J. Krawczyk, J. Kruczkowski, T. Pałka, Variability of the Velocity Field and Volumetric Flow Rate in Air Ways of Underground Mines. Archives of Mining Sciences, Kraków 1 (2006).

[20] J. Krawczyk, Single and multiple-dimensional models of unsteady air and gas flows in underground mines. Monograph, Strata Mechanics Research Institute of Polish Academy of Science (2007).

[21] J. Kruczkowski, J. Krawczyk, P. Ostrogórski, Laboratory investigations of stationary methane anemometer. Archives of Mining Sciences **62** (2017).

[22] F. Menter, Turbulence Modeling for Engineering Flows. ANSYS Inc. (2012).

[23] B. Mitka, P. Klapa, P. Pióro, Acquisition and Processing Datafrom UAVs in the Process ofGenerating 3D Models for SolarPotential Analysis. Remote Sens. **15**, 1498, (2023). DOI: https://doi.org/10.3390/rs15061498

[24] M. Nadeem, J.H. Lee, J. Lee, H.J. Sung, Turbulent boundary layers over sparsely-spaced rod-roughened walls. International Journal of Heat and Fluid Flow **56** (2015).

[25] J. Pokorný, L. Brumarová, P. Kučera, J. Martinka, A. Thomitzek, P. Zapletal, The effect of Air Flow Rate on Smoke Stratification in Longitudinal Tunnel Ventilation. Acta Montanistica Slovaca **24**, 3 (2019).

[26] T. Roszkowski, W. Trutwin, J. Wacławik, Mine ventilation measurements. Wydawnictwo "Śląsk", Katowice (1992).

[27] P. Skotniczny, P. Ostrogórski, Three-dimensional air velocity distributions in the vicinity of a mine heading's sidewall. Archives of Mining Sciences **63**, 2 (2018).

[28] V. Sokoła-Szewioła, J. Wiatr, Application of laser scanning method for the elaboration of digital spatial representation of the shape of underground mining excavation. Przegląd Górniczy **8** (2013)

[29] M. Štroner, T. Křemen, J. Braun, R. Urban, P. Blistan, L. Kovanič, Comparison of 2.5D Volume Calculation Methods and Software Solutions, Using Point Clouds Scanned Before and After Mining. Acta Montanistica Slovaca **24**, 4 (2019).

[30] S. Trenczek, A. Lutyński, A. Dylong, P. Dobrzeniecki, Controlling the longwall coal mining process at a variable level of methane hazard, Acta Montanistica Slovaca **25**, 2 (2020).

[31] M.A. Wala, S. Vytla, C.D. Taylor, G. Huang, Mine face ventilation: a comparison of CFD results against benchmark experiments for the CFD code validation. Mining Engineering (2007).

[32] K. Wierzbiński, Wpływ geometrii chodnika wentylacyjnego i sposobu jego likwidacji na rozkład stężenia metanu w rejonie wylotu ze ściany przewietrzane sposobem U w świetle obliczeń numerycznych CFD. (in Polish) Zeszyty Naukowe Instytutu Gospodarki Surowcami Mineralnymi i Energią Polskiej Akademii Nauk 94 (2016).

[33] H. Yi, M. Kim, D. Lee. Park, J. Applications of Computational Fluid Dynamics forMine Ventilation in Mineral Development. Energies **15**, 8405 (2022). DOI: https://doi.org/10.3390/en15228405

[34] M. Zagarola, Mean-flow scaling of turbulent pipe flow. Ph.D. thesis, Princeton University (1996).